Proceedings of the ICBBG2025
2025 International conference on Bio-mediated and Bio-inspired Geotechnics
18-20 May, 2025 | Tempe, Arizona, USA
https://doi.org/10.53243/ICBBG2025-147

Mechanical Characterization of Bacteria-Encapsulated Hydrogels for Enhanced Microbial-Induced Carbonate Precipitation (MICP)

Mert Kavala[1], Cambry Stratton[2], Berkin Dortdivanlioglu[3], Alexandra Clarà Saracho[4]

[1] Department of Civil, Architectural and Environmental Engineering, The University of Texas at Austin, 301E E Dean Keeton St c1700, Austin, TX 78712, United States.
E-mail: mertkavala@utexas.edu
[2] Department of Civil, Architectural and Environmental Engineering, The University of Texas at Austin, 301E E Dean Keeton St c1700, Austin, TX 78712, United States.
E-mail: strattoncambry@gmail.com
[3] Department of Civil, Architectural and Environmental Engineering, The University of Texas at Austin, 301E E Dean Keeton St c1700, Austin, TX 78712, United States.
E-mail: berkin@utexas.edu
[4]Department of Civil, Architectural and Environmental Engineering, The University of Texas at Austin, 301E E Dean Keeton St c1700, Austin, TX 78712, United States.
E-mail: alexandra.clara.saracho@utexas.edu

ABSTRACT

Creating multifunctional soft materials that enable controlled microbially induced calcium carbonate precipitation (MICP) with good mechanical properties is key to addressing geotechnical challenges such as soil stabilization and carbon storage. We have previously demonstrated a competitive displacement strategy to control the location and timing of the MICP reaction by immobilizing *Sporosarcina pasteurii* within biocompatible alginate hydrogel capsules. Here, we investigate the effect of gelling time and gelling agent concentration on the mechanical performance of hydrogel composites, as well as the behavioral changes of hydrogel capsules during MICP reactions. Notably, submillimeter-sized capsules were subjected to cyclic compression tests, enabling the real-time characterization of $CaCO_3$ stiffness evolution during MICP. The aqueous chemistry was monitored using spectrophotometric analysis during gel liquefaction and ureolysis. These findings will help define key manufacturing parameters to improve soil-hydrogel compatibility and support the practical use of biomineral composites in soils.

INTRODUCTION

Microbial-induced calcium carbonate ($CaCO_3$) precipitation (MICP) by ureolysis leading to the formation of $CaCO_3$ minerals has gained attention due to its ability to modify soil properties for geotechnical applications, such as soil stabilization (van Paasen et al. 2010; Montoya et al. 2014), erosion control (Jiang & Soga 2017; Saracho et al. 2021a), and carbon capture and storage (Okyay et al. 2016; Saracho & Marek 2024). MICP is influenced by multiple parameters that make its standardization in soils difficult, including particle shape and size of the treated soil (Mitchell & Santamarina 2005), ambient temperature and pH (Lauchnor et al. 2015), and viability and type of microbial strain used (Whiffin 2004; Saracho et al. 2020). As a result, the quantity, location, and

structure of the precipitates, and hence, mechanical properties, are governed by both intrinsic factors (*e.g.*, ion concentrations, surface charge) and extrinsic factors (*e.g.*, pH, temperature, ionic strength). This variability underscores the need for standardized and broadly applicable treatment methods that ensure consistent performance (Fu et al. 2023; Tang et al. 2020).

In bioaugmentation, where exogenous microorganisms are introduced into the soil, bacterial encapsulation can help overcome some of these challenges by facilitating storage and transportation, dispersibility, and controlled release of MICP (Saracho et al. 2021b). Alginate hydrogels are particularly suitable as they contain a high-water content, and are non-toxic, biocompatible, and biodegradable. The gelation mechanism of alginate, known as the egg-box model, occurs when alginate chains are crosslinked by divalent cations, such as calcium (Ca^{2+}) (Fang et al. 2007). Hence, competitive displacement of the chelated ions can be used to liquefy the gel. More specifically, calcium-binding properties in yeast extract, such as glutamate and aspartate, exhibit a pH-dependent ion affinity that can be exploited to harvest the calcium ions that crosslink alginate, and hence trigger the release of immobilized bacteria (Saracho et al. 2021b). While studies have examined the mechanical properties of soil-gel scaffolds (Wen et al. 2019; Heveran et al. 2020) and the micro-mechanical properties of hydrogel beads (Mattei et al. 2017), how and to what extent the micro-mechanical behavior of bacteria-laden hydrogel beads changes during MICP remains unknown. Yet, this is important because understanding the micro-mechanical behavior of bacteria-laden hydrogel beads during MICP is crucial for optimizing the controlled release of bacteria and predicting treatment outcomes in soil. This will advance our ability to design more efficient and reliable soil improvement techniques.

This study examines the biochemical reactions and micro-mechanical changes during the transformation of hydrogel droplets, which can be as strong as sand beads (Pungrasmi et al., 2019), into $CaCO_3$ precipitates. This transformation was monitored spectrophotometrically by tracking pH changes during gel liquefaction and MICP. For the first time, we employed micro-scale compression-relaxation tests to quantify the temporal evolution of Young's modulus in precipitated calcium carbonate during MICP, revealing a remarkable increase in stiffness.

METHODOLOGY

Bacterial growth and pellet preparation. *Sporosarcina pasteurii* (ATCC 11859) is a gram-positive strain with high urease enzyme activity, which plays a significant role in calcium carbonate precipitation. Bacteria from 25% glycerol stocks at -80°C were inoculated on ATCC 1376 agar plates (13 mM tris buffer, 20.0 g/l yeast extract, 10 g/l ammonium sulfate, and 20.0 g/l agar, Sigma-Aldrich, pH 9.0) and incubated at 30°C for 48 hours. Single colonies were subsequently resuspended and incubated in ATCC 1376 liquid medium for approximately 12 hours at 30 °C and 200 rpm until they reached the mid-exponential phase (approximately $5x10^8$ CFU/mL). Finally, bacterial pellets were obtained by centrifuging the bacterial cultures at 4800 rpm for 10 minutes at 4 °C, washing with phosphate-buffered saline (1x, Sigma-Aldrich), and centrifuging again to remove any remaining growth media components.

Immobilisation of *S. pasteurii* in hydrogel beads. Alginate was used as supporting hydrogel at concentrations of 2.0%, 3.0%, and 3.6% w/v. Hydrogel solutions were mixed with bacterial pellets (1.5% w/v) and homogenized with a magnetic stirrer. A calcium-mediated gelling bath was used, prepared by dissolving 1.0 M calcium chloride ($CaCl_2$) in Milli-Q water and sterile-filtered (0.2µm). The extrusion setup consists of an infusion pump (Harvard Apparatus PhD Ultra) loaded

with a syringe containing the alginate-bacteria solution. This syringe was connected to a vertically clamped precision needle (25 G), with the magnetically stirred gelling bath positioned underneath. The distance between the needle tip and the surface of the gelling bath was set to 5 cm. The dripped beads were stirred for 30 minutes to facilitate cross-linking, then rinsed with Milli-Q water, and stored in Milli-Q water at 4°C until further use.

Control of ureolysis and mineral precipitation and monitoring of ureolysis. Calcium-binding peptides in yeast extract display a pH-dependent ion affinity, which can be utilized to chelate the calcium ions that crosslink alginate, thereby triggering the release of the immobilized bacteria (Clarà Saracho et al., 2021b). The calcium-binding affinity of some of the proteins and peptides in yeast extract increases at high pH, while alginate's decreases. This can be exploited to liquefy the alginate beads by putting them in contact with a high-pH urea and yeast extract solution (pH 10) triggering the release of MICP over a 24-hour period.

To independently assess gel liquefaction, ureolysis, and $CaCO_3$ precipitation tests were performed using three different triggering solutions, all based on the same YE-pH9.8 (Yeast Extract, pH 9.8) solution. This base solution was prepared with phenol red as a pH indicator for photometric monitoring, Tris base as a pH buffer, and yeast extract as the source of calcium-binding peptides. Additionally, YE (pH 9.8) was prepared with 1 M urea, and equimolar amounts of urea and $CaCl_2$ (1M), as listed in Table 1. Bacterial and non-bacterial (control) hydrogel beads were placed in 300 μL of the triggering solution in 96-well plates. Measurements were taken every minute over a 24-hour period at constant temperature using a plate reader (Biotek Synergy Neo 2) at the peak absorbance of the pH indicator (560 nm). A560 readings were then converted to the corresponding pH values using the standard curve shown in Figure 1, with equations describing the linear relationship between A560 and pH across different pH intervals. The YE-pH9.8 (1M urea 1M $CaCl_2$) solution was excluded due to the interference of the precipitation with the absorbance measurements.

Table 1. Chemical compositions of the triggering solutions

Test ID	Yeast Extract (YE), $g \cdot L^{-1}$	Tris base, M	Urea, M	Calcium chloride ($CaCl_2$), M	Phenol red $g \cdot L^{-1}$
YE-pH9.7	3	0.13 M	-	-	0.01
YE-pH9.7 (1M Urea)	3	0.13 M	1	-	0.01
YE-pH 9.7 (1M Urea 1M $CaCl_2$)	3	0.13 M	1	1	0.01

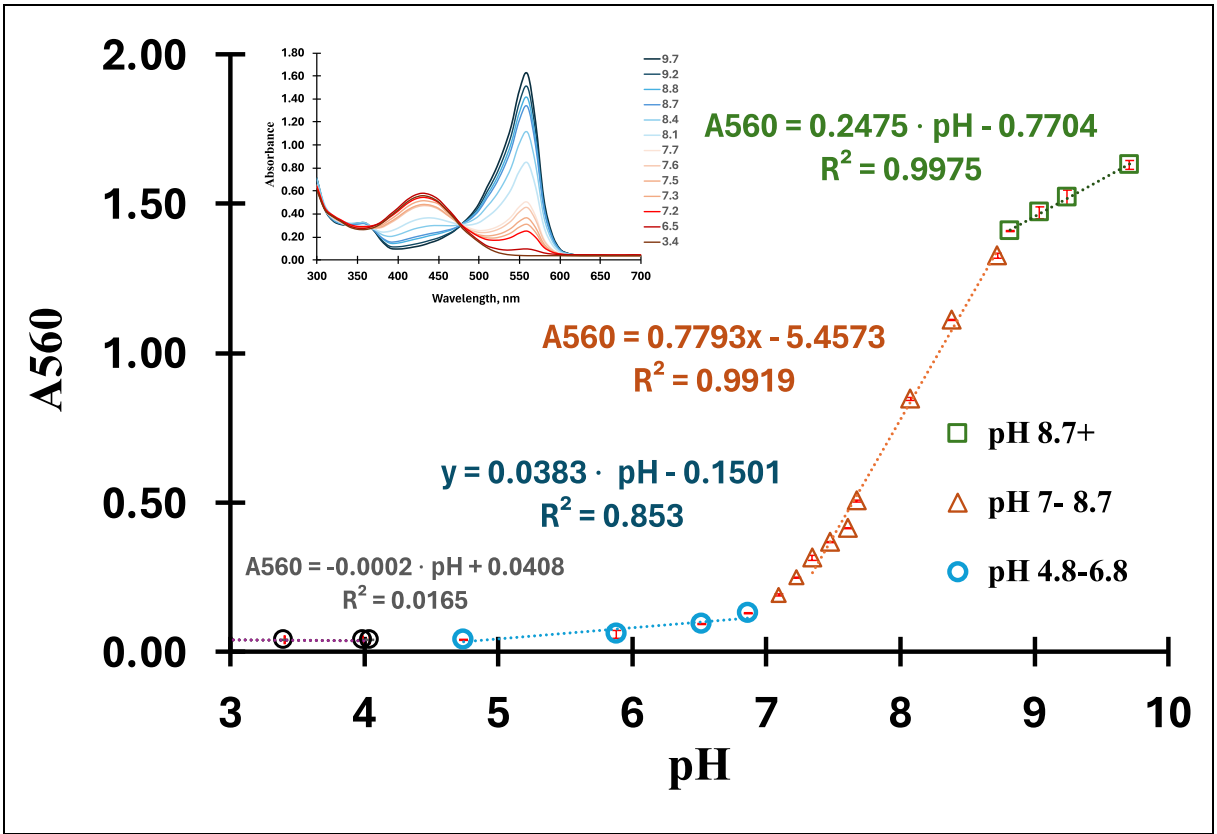

Figure 1. Calibration curve for pH analysis using phenol red, with inset showing the absorbance spectra of phenol red. The values are expressed as the mean ± standard deviation (SD) based on triplicate measurements.

Micromechanical testing of hydrogel beads. Compression-tension experiments on submillimeter hydrogel beads were carried out using the Microtester G2 (Cell Scale), a micro-scale biomaterials testing device that uses a piezoelectric actuator with 0.1 µm resolution. Tested hydrogels were placed in a bath filled with either sterile DI water or one of the three triggering solutions listed in Table 1. DI was used to evaluate the effect of alginate concentration on non-liquefied beads. The circular tungsten microbeam with a diameter of 1.0160 mm was attached to a platen, and then was positioned at the topmost point of the hydrogel bead prior to testing. Following MICP, samples become significantly stiffer and brittle, and thus, a low axial strain (5%) was selected across all tests to ensure consistent testing conditions. Repeated loading and unloading cycles were applied at a rate of 300s under a constant displacement rate, and strain was computed from high-resolution charge-coupled device (CCD) imaging.

RESULTS AND DISCUSSION

Chemical effects of components in the triggering solution on the hydrogel beads. To observe the biotic and abiotic effects of gel liquefaction and ureolysis, pH levels were monitored over 24 hours after the hydrogel beads were placed in the solutions, as shown in Figure 2. Figure 2a and 2b show the results for gel samples with and without bacteria in YE-pH9.8 and YE-pH9.8 (1M urea) solutions. The figures also include results for a sample containing only a bacterial pellet,

equivalent to the total bacterial mass in one gel but without the gel itself. As expected, no gel liquefaction occurred in DI water, with pH remaining stable at 7. In contrast, samples placed in YE-pH9.8 showed an initial pH drop within the first 4 hours, attributed to the release of calcium ions from the gels, as shown in Figure 2a. This was followed by stabilization, indicates that the solution has a buffering capacity, allowing the pH to stabilize again, with a slight continued decrease in pH observed afterward for even the sample with no gel.

In samples with YE-pH9.8 (1M urea), ureolysis drives pH changes towards the pKa of ammonium. Based on the initial pH of the YE-pH9.8 (1M urea), pH levels are expected to decrease as ureolysis proceeds, leading to an increase in the concentration of carbonate ions. The Ca^{2+} released from the gels subsequently enables the precipitation of $CaCO_3$, further reducing pH. However, due to the limited calcium source, precipitation around the gel was not sufficient to prevent bacterial release. Instead, the presence of urea maintained a suitable pH, while factors such as nutrients and temperature create a suitable environment for bacterial growth and ureolysis.

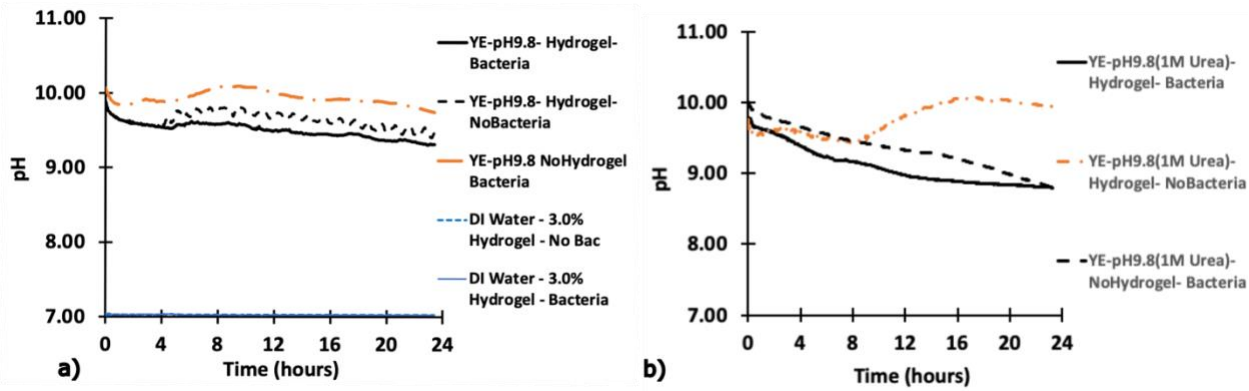

Figure 2. Changes in pH of bacterial and non-bacterial samples in a) DI-water and YE-pH9.8, and b) YE-pH9.8 (1M urea) triggering solutions

Effect of alginate concentration and gelling time in the mechanical behavior of hydrogel beads. Beads with 3.0% w/v alginate concentration and 3.6% w/v alginate concentration exhibited a spherical geometry with sphericity factors of 0.017 (n=5, ±0.005) and 0.033 (n=10, ±0.010), both below the spherical threshold of 0.05 calculated using Equation 2. This sphericity factor, determined by the ratio of maximum (d_{max}) and minimum (d_{min}) diameters.

$$\textit{Sphericity Factor (SF)} = \frac{d_{max} - d_{min}}{d_{max} + d_{min}} \text{ (Chen et. al. 2009)} \qquad \textbf{(2)}$$

The mechanical behavior of hydrogel beads was systematically evaluated through compression-relaxation experiments conducted under controlled conditions. The tests involved three successive loading-unloading cycles at 5% maximum strain, with the beads immersed in DI water. The elastic modulus demonstrated a strong linear correlation with alginate concentration as shown in Figure 3a, following the relationship Equation 3. The extension of gelation time from 30 to 120 minutes showed no significant impact on the elastic modulus, maintaining consistent values around 75-80 kPa for 3.0% (w/v) hydrogel as shown in Figure 3b. This observation suggests that the cross-linking process reaches completion within the initial 30-minute period.

The stress-strain curve for 3% alginate beads demonstrated complete elastic recovery after

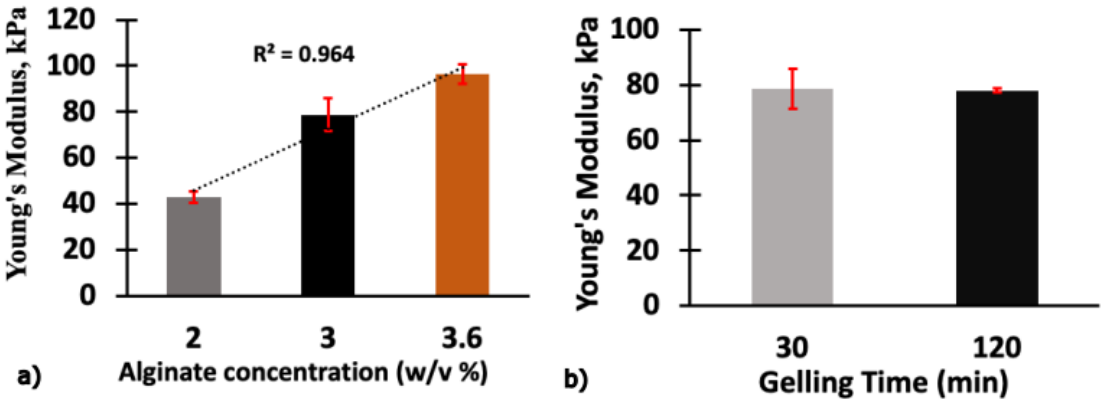

Figure 3. a) effect of alginate concentration on the elastic modulus, and b) effect of gelling time on the elastic modulus.

$$\boldsymbol{Elastic\ modulus, E\ (kPa)} = \mathbf{26.851}\ [\boldsymbol{Alginate}]\ (\%) + \mathbf{18.941} \quad (R^2 = 0.964) \quad \textbf{(3)}$$

relaxation, with an average Young's modulus of 78.6 kPa and reaching a maximum stress of 676 N/m² at 5% strain as shown in Figure 4a and Figure 4b. Similarly, beads with 3.6% alginate concentration exhibited elastic behavior with a higher Young's modulus of 96.5 kPa. This is in agreement with Moe et al. (1992), who reported a similar viscoelastic behavior of cubic Ca-alginate ethanol gels. The measured stresses during testing are below the ultimate strength of the hydrogel beads.

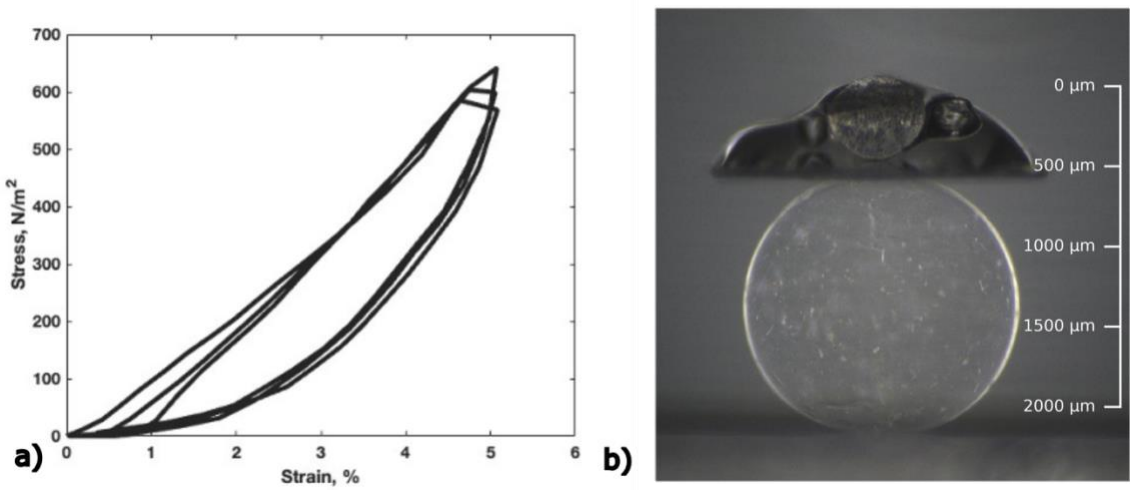

Figure 4. a) Stress-strain plot of 3% hydrogel bead b) image of hydrogel bead after relaxation.

Mechanical characterization of bacteria-encapsulated hydrogels. A 5% compression-relaxation test was performed on bacteria-laden hydrogel beads (3.6% w/v) immersed in DI water

and YE-pH9.8 (1M urea and 1M $CaCl_2$) triggering solution. Tests in the triggering solution showed a 3-fold increase in Young's modulus over time due to MICP, as shown in Figure 5a. $CaCO_3$ precipitation primarily occurred within the hydrogel bead due to the local supersaturation offered by the release of Ca^{2+} (Figure 5b). The 24-hour test could not be completed because the bead collapsed under the first loading cycle. The observed decrease in Young's modulus at the 19th hour relative to the 7th hour is attributed to cumulative irreversible deformation, resulting from the precipitation of $CaCO_3$ and the progressive expansion of microcracks induced by repeated loading cycles.

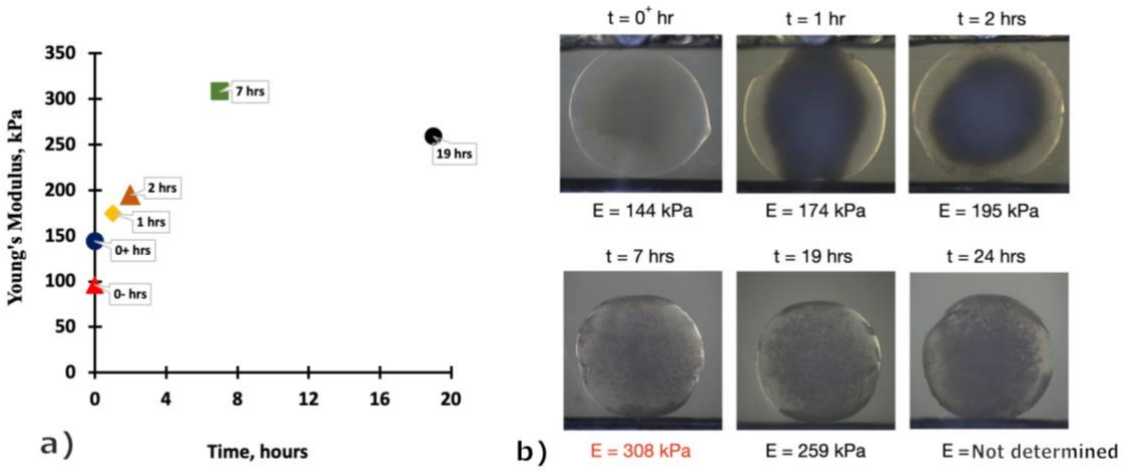

Figure 5. 5% compression relaxation test results of bacteria-encapsulated hydrogel in triggering solution. a) images over time and b) changes in Young's modulus over time.

CONCLUSION

This study examines the changes in pH and micro-mechanical behavior of bacteria-laden hydrogel beads to better understand their role in facilitating controlled bacterial release and the progression of MICP as a soil improvement technique. Taking advantage of the calcium binding affinity of certain amino acids present in yeast extract, we used a peptide-responsive release mechanism that makes the calcium ions that are weakly bound to the hydrogel matrix readily available for $CaCO_3$ precipitation. To capture gel liquefaction and ureolysis, pH was monitored spectrophotometrically over time in triggering solutions with varying chemical compositions. The effect of key manufacturing parameters, such as alginate concentration and gelling time, on the Young's modulus of hydrogel beads was illustrated and mathematically expressed. For the first time, the evolution of $CaCO_3$ Young's modulus during MICP was characterized using micro-scale compression-relaxation tests, revealing a 3-fold increase in stiffness over a 7-hour period. These findings provide valuable insights into hydrogel bead design and real-time monitoring of key parameters during MICP, offering a robust framework to optimize biomineral composite applications.

REFERENCES

Chan, E. S., Lee, B. B., Ravindra, P., & Poncelet, D. (2009). Prediction models for shape and size of ca-alginate macrobeads produced through extrusion–dripping method. Journal of colloid and interface science, 338(1), 63-72.

Chan, E. S. (2011). Preparation of Ca-alginate beads containing high oil content: Influence of process variables on encapsulation efficiency and bead properties. Carbohydrate polymers, 84(4), 1267-1275.

Clarà Saracho, A., Haigh, S. K., Hata, T., Soga, K., Farsang, S., Redfern, S. A., & Marek, E. (2020). Characterisation of CaCO3 phases during strain-specific ureolytic precipitation. Scientific Reports, 10(1), 10168.

Clarà Saracho, A., Haigh, S. K., & Ehsan Jorat, M. (2021a). Flume study on the effects of microbial induced calcium carbonate precipitation (MICP) on the erosional behaviour of fine sand. Géotechnique, 71(12), 1135-1149.

Clarà Saracho, A., & Marek, E. J. (2024). Uncovering the Dynamics of Urease and Carbonic Anhydrase Genes in Ureolysis, Carbon Dioxide Hydration, and Calcium Carbonate Precipitation. Environmental Science & Technology, 58(2), 1199-1210.

Fang, Y., Al-Assaf, S., Phillips, G. O., Nishinari, K., Funami, T., Williams, P. A., & Li, L. (2007). Multiple steps and critical behaviors of the binding of calcium to alginate. The Journal of Physical Chemistry B, 111(10), 2456-2462.

Fu, T., Saracho, A. C., & Haigh, S. K. (2023). Microbially induced carbonate precipitation (MICP) for soil strengthening: A comprehensive review. Biogeotechnics, 1(1), 100002.

Heveran, C. M., Williams, S. L., Qiu, J., Artier, J., Hubler, M. H., Cook, S. M., ... & Srubar, W. V. (2020). Biomineralization and successive regeneration of engineered living building materials. Matter, 2(2), 481-494.

Jiang, N. J., & Soga, K. (2017). The applicability of microbially induced calcite precipitation (MICP) for internal erosion control in gravel–sand mixtures. Géotechnique, 67(1), 42-55.

Lauchnor, E. G., Topp, D. M., Parker, A. E., & Gerlach, R. (2015). Whole cell kinetics of ureolysis by Sporosarcina pasteurii. Journal of applied microbiology, 118(6), 1321-1332.

Mattei, Giorgio, Ludovica Cacopardo, and Arti Ahluwalia. "Micro-mechanical viscoelastic properties of crosslinked hydrogels using the nano-epsilon dot method." Materials 10, no. 8 (2017): 889.

Moe, S. T., Draget, K. I., Skjåk-Bræk, G., & Simdsrød, O. (1992). Temperature dependence of the elastic modulus of alginate gels. Carbohydrate polymers, 19(4), 279-284.

Mitchell, J. K., & Santamarina, J. C. (2005). Biological considerations in geotechnical engineering. Journal of geotechnical and geoenvironmental engineering, 131(10),

Montoya, B. M., DeJong, J. T., & Boulanger, R. W. (2014). Dynamic response of liquefiable sand improved by microbial-induced calcite precipitation. In Bio-and chemo-mechanical processes in geotechnical engineering: Géotechnique symposium in print 2013 (pp. 125-135). ICE Publishing.

Nikbakhtan, B., & Osanloo, M. (2009). Effect of grout pressure and grout flow on soil physical and mechanical properties in jet grouting operations. International Journal of Rock Mechanics and Mining Sciences, 46(3), 498-505.

Okyay, T. O., Nguyen, H. N., Castro, S. L., & Rodrigues, D. F. (2016). CO2 sequestration by ureolytic microbial consortia through microbially-induced calcite precipitation. Science of the Total Environment, 572, 671-680.1222-1233

Pungrasmi, W., Intarasoontron, J., Jongvivatsakul, P., & Likitlersuang, S. (2019). Evaluation of microencapsulation techniques for MICP bacterial spores applied in self-healing concrete. Scientific reports, 9(1), 12484.

Saracho, A. C., Lucherini, L., Hirsch, M., Peter, H. M., Terzis, D., Amstad, E., & Laloui, L. (2021b). Controlling the calcium carbonate microstructure of engineered living building materials. Journal of Materials Chemistry A, 9(43), 24438-24451.

Tang, C. S., Yin, L. Y., Jiang, N. J., Zhu, C., Zeng, H., Li, H., & Shi, B. (2020). Factors affecting the performance of microbial-induced carbonate precipitation (MICP) treated soil: a review. Environmental Earth Sciences, 79, 1-23.

Wu, Y., Li, H., & Li, Y. (2021). Biomineralization Induced by Cells of Sporosarcina pasteurii: Mechanisms, Applications and Challenges. Microorganisms, 9(11), 2396.

van Paassen, L. A., Ghose, R., van der Linden, T. J., van der Star, W. R., & van Loosdrecht, M. C. (2010). Quantifying biomediated ground improvement by ureolysis: large-scale biogrout experiment. Journal of geotechnical and geoenvironmental engineering, 136(12), 1721-1728.

Wen, K., Li, Y., Huang, W., Armwood, C., Amini, F., & Li, L. (2019). Mechanical behaviors of hydrogel-impregnated sand. Construction and Building Materials, 207, 174-180.

Whiffin, V. S. (2004). Microbial CaCO3 precipitation for the production of biocement (Doctoral dissertation, Murdoch University).

Yin, J. H., & Zhou, W. H. (2009). Influence of grouting pressure and overburden stress on the interface resistance of a soil nail. Journal of Geotechnical and Geoenvironmental Engineering, 135(9), 1198-1208.